CROATICA CHEMICA ACTA CCACAA 57 (6) 1355—1370 (1984)

CCA-1527

YU ISSN 0011-1643
UDC 541
Original Scientific Paper

The Bonding of P_4 to d^8-ML_3 Complexes

Sung-Kwon Kang, Thomas A. Albright[*1a], and Jerome Silvestre*[1b]

Department of Chemistry, University of Houston, Houston, Texas 77004, USA

Received February 3, 1984

Extended Hückel calculations were carried out on η^1, η^2, and η^3 complexes of P_4 to $Rh(PH_3)_2Cl$. The η^1-square planar and an η^2 complex with C_{2v} symmetry are the most stable. Geometrical optimizations and a detailed account of the bonding in each have been carried out. d^{10} η^1-tetrahedral complexes of P_4 are expected to be quite stable. The best candidate for an η^3 mode of bonding is the trimer $Fe_3(CO)_9$. Alternative complexes at η^3 include a d^6-ML_3 and d^4-ML_4 species, however reactivity problems in the former and steric constraints in the latter may prohibit their isolation.

There have been a number of compounds recently prepared and structurally determined of the $\eta^3-P_3-ML_3$ and $\eta^3-P_3-M_2L_6$ type.[2,3] These are usually made by reaction of white phosphorus with a labile transition metal complex. Several other P_n »clusters« coordinated to a transition metal are known, however, many are not well categorized at the present time. Intact Ni and Pd complexes of P_4 have been prepared using the tris (2-diphenylphosphinoethyl)amine chelate.[2b,5] The structure[5] of the Ni complex shows it to be an η^1 complex, as shown in **1**. What initialy caught our attention and

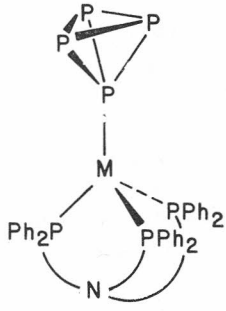

1

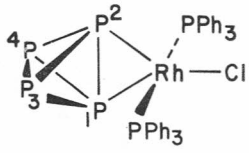

2

provided the impetus for this work was the report[6] that d^8-$M(PR_3)_2X$ complexes of P_4 could be isolated where M=Rh, Ir; X=Cl, Br, I. Most importantly, the ^{31}P spectrum of $Rh(P_4)(PPh_3)_2Cl$ was an $A_2B_2M_2X$ spin system[6a] which implies either a static structure of C_{2v} symmetry or a rapidly equilibrating

one which averages to a structure of this symmetry. The spectra remain unchanged over a temperature range of —70 °C to +40 °C, thus it was reasonble to postulate a novel η^2 type of coordination, as shown in **2**. Very recently the structure of $Rh(P_4)(PPh_3)_2Cl$ was determined[7] which indeed does show an η^2 coordination mode for the P_4 unit, and preliminary extended Hückel calculations were carried out to examine the bonding in the complex. We were interested in what geometrical factors favored the formation of an η^2 geometry over a normal 16 electron, η^1-square planar isomer. Furthermore, we wondered whether or not an η^1-tetrahedral or η^3-piano stool were viable possibilities in this or other electron counts.

A series of extended Hückel calculations were carried out on $Rh(P_4)(PH_3)_2Cl$ for the isomers shown in **3**—**7**. Here all P—P distances in P_4 were fixed at 2.21 Å; the value of the isolated molecule.[8] The other pertinent geometrical

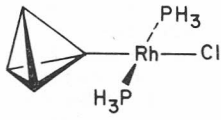

(0)

3

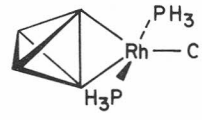

(37)

4

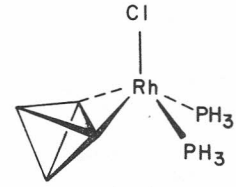

(53)

5

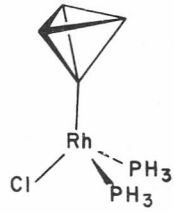

(41)

6

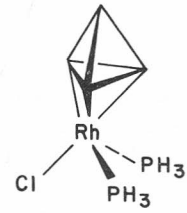

(81)

7

details and parameters are listed in the Appendix. The relative energies (in kcal/mol) are listed in parenthesis under each structure. Surprisingly the η^1-square planar structure, **3**, is computed to be 37 kcal/mol *more* stable than the correct η^2 isomer, **4**. Before we discuss the bonding and geometrical optimizations performed on **3** and **4**, it is worthwhile to digress for a moment and derive the valence orbitals of the P_4 fragment.

The P_4 Fragment Orbitals

There have been several previous theoretical studies[9] of P_4. Perhaps the easiest way to construct the valence orbitals of this cluster starts by artifically partitioning the orbitals on each phosphorus atom into three types. Firstly, each atom contains one *sp* hybrid which is pointed towards the center of the tetrahedron, as shown by **8** in Scheme I. These four radial orbitals form

SCHEME I

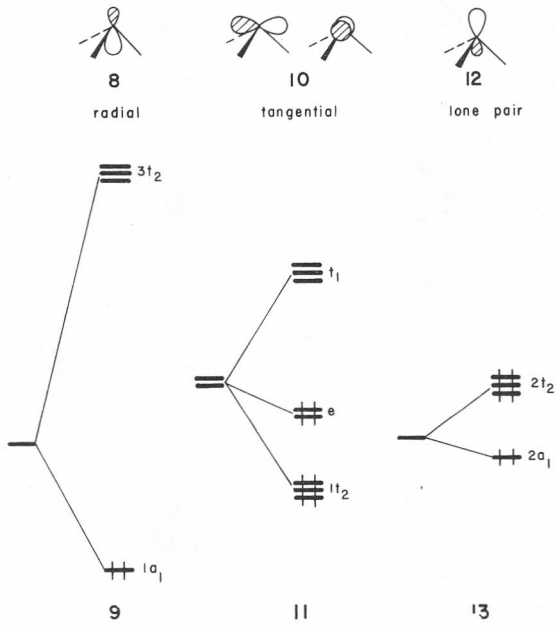

bonding ($1a_1$) and antibonding ($3t_2$) molecular orbitals, see **9**. Since the overlap is large between the radial hybrids, the $1a_1$ and $3t_2$ molecular orbitals are split by a large amount. Each phosphorus atom also uses two atomic p orbitals, **10**, for tangential bonding. The overlap here is less than that for the radial types so the $1t_2+e+t_1$ members of the tangential set are not seperated in energy as much as the radial set. Finally each phosphorus will have an sp hybrid pointed away from the cluster, **12**. These lone pairs will have an even smaller overlap with each other. Therefore, the $2a_1+2t_2$ set is split to a very small extent in **13**. Notice that the radial, tangential, and lone pair functions each yield one t_2 set. Unfortunately there is some intermixing between them, but the level ordering and *basic* composition is retained in an extend Hückel calculation. With 20 valence electrons $2t_2$ is the HOMO and t_1 is the LUMO.

The t_1, $2t_2$, e, and $2a_1$ molecular orbitals will figure heavily into our discussion; they are presented in two ways in Figure 1. On the left side of Figure 1 these orbitals are displayed in manner convenient for interaction with a ML_3 fragment *via* edge-bonding (η^2). Intermixing of tangential character from the $1t_2$ set into $2t_2$ is evident. On the right side of Figure 1 the valence orbitals of P_4 are drawn for η^1 and η^3 bonding. Each member of t_1, $2t_2$, and e have been individually labeled to facilitate our discussion. Different linear combinations have been taken for the $2t_2$ set on the left and right sides of Figure 1. This will simply their interactions with the ML_3 unit at the η^1, η^2, and η^3 geometries.

The reader should note that the low energy of the t_1 set and high energy of e make these orbitals good electron acceptors and donors, respectively. The

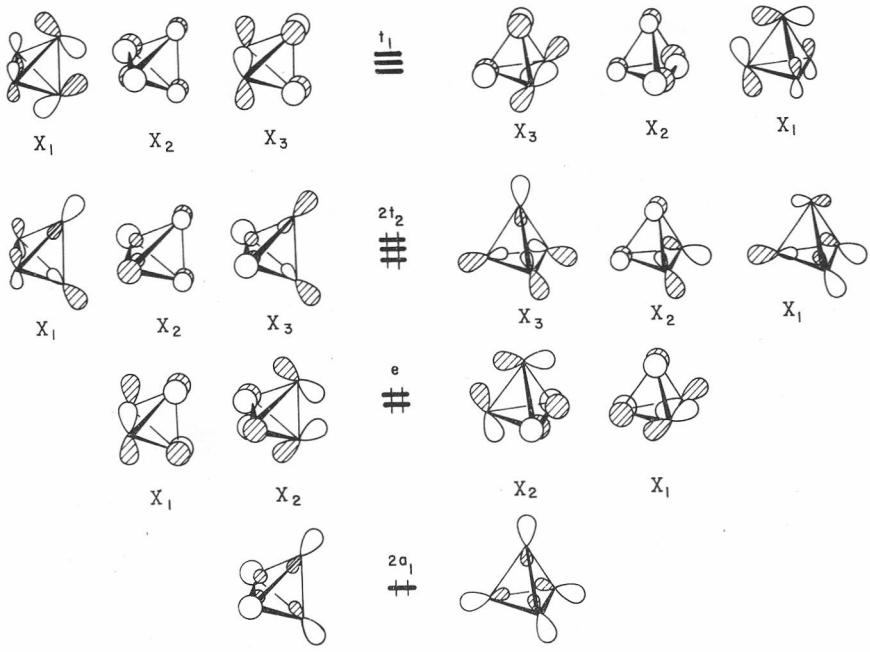

Figure 1. Two perspectives of the important valence orbitals in P_4.

lone pair combinations, $2a_1$ and $2t_2$, are pointed away from the vertices of the tetrahedron. Consequently their overlap with ML_3 at η^2 (on the edge of the tetrahedron) or η^3 (on a face) is expected to be small.

η^1 and η^2 Bonding to a C_{2v} ML_3 Fragment

Using an undistorted P_4 geometry the η^1 and η^2 coordination modes to a square planar $Rh(PH_3)_2Cl$ unit in **3** and **4** are computed to be more stable than the other conceivable geometries. Let us start our analysis with the η^1 geometry. The molecular orbitals are constructed for **3** in Figure 2. On the right side of this Figure are the orbitals of a C_{2v} ML_3 fragment.[10] At low energy are the four filled orbitals, $1a_1 + 1b_2 + b_1 + a_2$, associated with a square planar splitting pattern. The $1b_2$ and b_1 orbitals are pushed up somewhat in energy from a_2 because of antibonding from the C1 ligand. At higher energy the $2a_1$ fragment orbital is primarily the metal-ligand antibonding $x^2 - y^2$ level. However, it is also hybridized by metal s and p character towards the missing fourth ligand in a square planar complex.[10] Finally, at higher energy is an empty metal p orbital, $2b_2$. The $2a_1$ and χ_3 of $2t_2$ lone pair levels interact strongly with the $2a_1$ hybrid on ML_3 and are stabilized. This forms the principal source of bonding in this complex.

We also find that there is some back donation of electron density from the filled $1b_2$ and b_1 fragment orbitals of ML_3 into the empty members of t_1 (χ_2 and χ_3, respectively). It was computed that 0.16 and 0.14 electrons are transfered from $1b_2$ and b_1, respectively, to the members of t_1. This means that the Rh—P distance of P_4 should be shorter than normal. Furthermore, since t_1 is antibonding between the phosphorus atom coordinated to Rh and

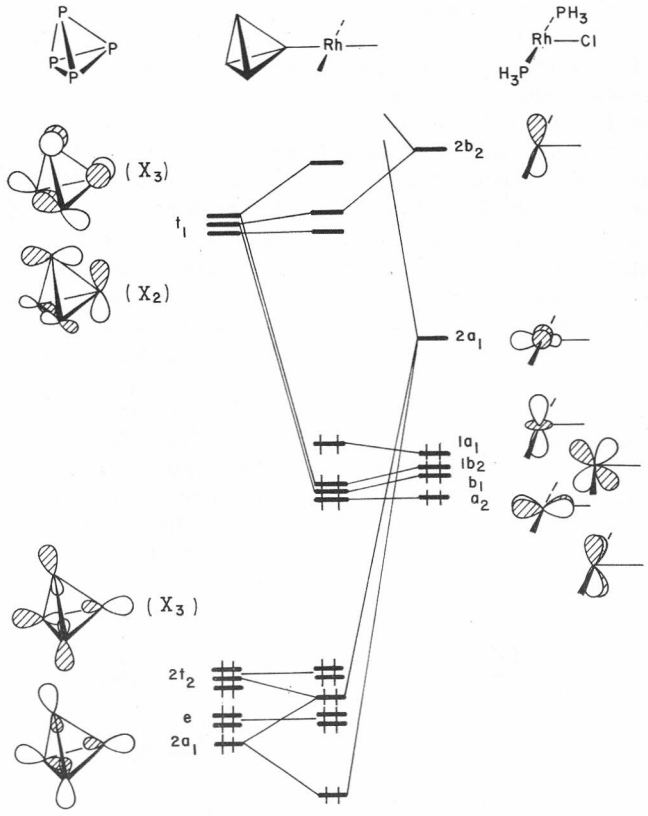

Figure 2. An orbital interaction diagram for the η^1-square planar geometry.

the other three basal phosphorus atoms, these P—P distances should increase. These distortions do indeed occur for the η^1-tetrahedral complex, **1**,[5] and, as we shall show later, for precisely the same reasons. An optimization of the Rh—P and P—P distances was carried out on the η^1-square planar complex to check the predictions we have made. Using the numbering system shown in **14**, an independent optimization within a C_s symmetry constraint yielded P_1—P_2 and P_1—P_3 distances of 2.31 Å while those for P_2—P_3 (P_2—P_4) and

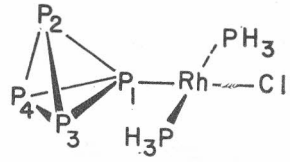

14

P_3—P_4 were found to be 2.10 Å. The Rh—P_1 distance was found to be too short — 1.85 Å. But given the approximate nature of the extended Hückel

method these results are encouragingly in the right direction. Finally, the H_3P—Rh—PH_3 was also varied in the optimization. We find that it is slightly bent back (170°) away from the P_4 unit for steric reasons.

The molecular orbitals for an η^2 complex using a T_d geometry for P_4 are constructed in Figure 3. Here there is essentially no overlap between χ_3 of the $2t_2$ set (see the left side of Figure 1) and $2a_1$ on P_4 with the $2a_1$ fragment orbital of ML_3. The latter fragment orbital is concentrated towards the bisector of the coordinated P—P bond while the lone pairs are directed away from it. Instead the χ_2 component of the e set on P_4 finds a good overlap with $2a_1$[11] and is stabilized to form the molecular orbital labeled a_1 in Figure 3. There are also π interactions at work between the P_4 and ML_3 fragments. In particular the $1b_2$ and $2b_2$ orbitals of ML_3 interact to a considerable extent with the χ_1 components of t_1 and $2t_2$. Three of the four resulting molecular orbitals are explicitly shown in Figure 3. The $1b_2$ fragment orbital on ML_3 overlaps with χ_1 on $2t_2$ and t_1 to approximately the same extent at this geometry; the magnitudes of the corresponding overlap integrals were 0.197 and 0.196, respectively. Notice that both $1b_2$ on ML_3 and χ_1 of $2t_1$ are filled. Thus, the interaction between them is repulsive. The antibonding combination between the two (the molecular orbital labeled $2b_2$) is kept at low energy only because of secondary mixings *via* χ_1 on t_1 and $2b_2$ on ML_3. Therefore,

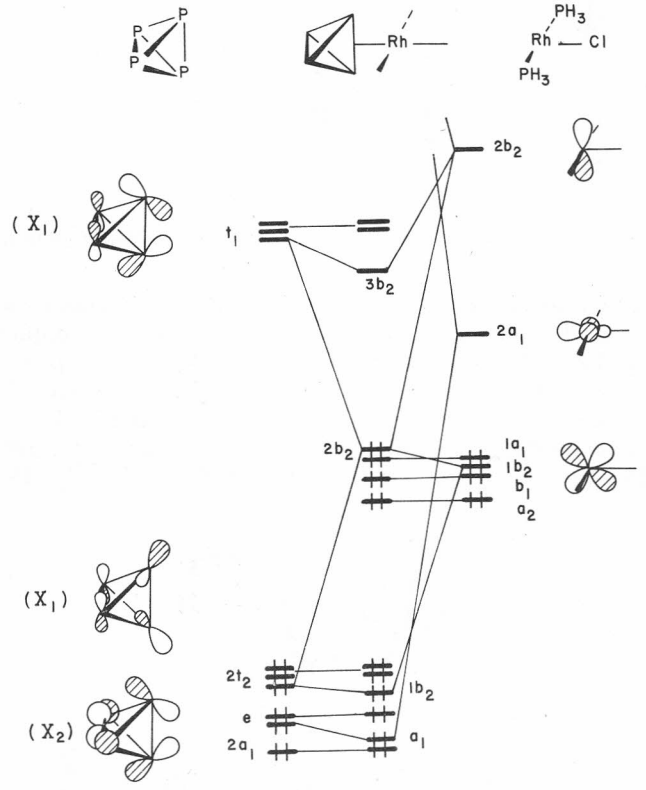

Figure 3. An orbital interaction diagram for the η^2 complex.

with an undistorted P_4 ligand it should come as no surprise that the η^1 complex is computed to be 37 kcal/mol more stable than η^2. There is much more efficient σ bonding at the η^1 geometry for overlap and energy gap reasons (the $2t_2$ set is higher in energy and closer to $2a_1$ than the e set is). Furthermore, there is little, if any, π stabilization in the η^2 species. Although no quantitive reliance should be placed on binding energies computed at this level, we find that the complex is *not* bound with respect to dissociation to P_4 and $Rh(PH_3)_2Cl$.

Careful inspection of Figure 3 shows that stabilization of the η^2-complex will be achieved by distorting the P_4 ligand so that the energy of χ_2 in the e set is raised, making it a better σ donor to the empty $2a_1$ level on ML_3. More importantly this distortion must lower the energy of χ_1 in the t_1 set so the backbonding from the filled $1b_2$ orbital on ML_3 is maximized. One way to achieve this is by elongating the P_1—P_2 bond (see the numbering system in **2** and **15**). A Walsh diagram for this distortion is given in Figure 4. Here Θ is defined as the P_1—P_3, P_4 bisector-P_2 angle shown in **15**. At the tetrahedral

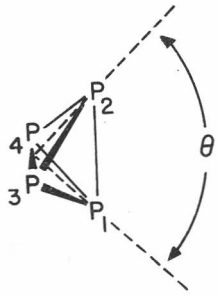

15

geometry $\Theta = 70.52°$. At larger angles the symmetry of the molecule is lowered to C_{2v}. The orbitals on the far right of Figure 4 have been relabeled to reflect this fact. Referring back to the valence orbitals of P_4 on the left side of Figure 1, nothing much happens to the orbitals of the $2t_2$ set and $2a_1$. Overlap between these hybrids within each component is small so they stay at relatively constant energy. The χ_1 component of the e set is stabilized as Θ increases. Antibonding between P_1 and P_2 is decreased while π bonding between P_1 and P_2 to P_3 and P_4 is increased. The χ_2 component of the e set is destabilized greatly since bonding between P_1 and P_2 is diminished. Actually this orbital along with χ_3 in the $2t_2$ set undergo a weakly avoided crossing (both become a_1 in symmetry). The resultant HOMO is drawn on the right side of Figure 4. The energetic variation of the individual members in t_1 can be derived in a similar fashion. Most importantly the χ_1 component which is strongly P_1—P_2 antibonding is tremendously stabilized as Θ increases. It becomes the LUMO of the molecule and its final form is also shown on the right of this Figure. For reference the energy of the two critical orbitals, $2a_1$ and $1b_2$, in the $Rh(PH_3)_2Cl$ fragment are indicated on the far left side of the Figure. In conclusion, increasing Θ raises the energy of $3a_1$ making it a better σ donor to the empty $2a_1$ fragment orbital on ML_3 and the energy of $2b_2$ is lowered making it a better π acceptor to the filled $1b_2$ orbital on ML_3.

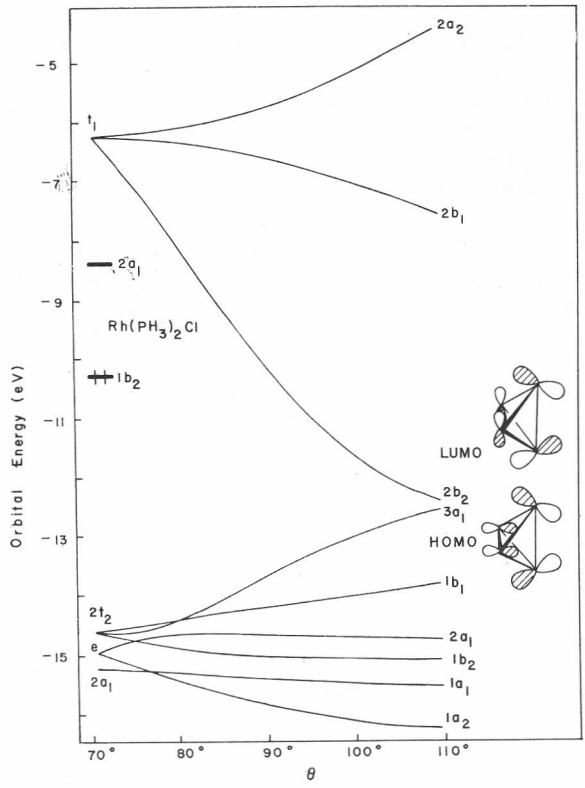

Figure 4. A Walsh diagram for elongating the P_1—P_2 bond (increasing Θ-see **15**) in P_4.

We optimized the P—P bond lengths, Rh—P bond lengths and H_3P—Rh—P angle within a C_{2v} symmetry constraint. Using the numbering system in **2** we find that in the optimized structure P_1—P_2 = 3.12 Å, P_2—P_3 (*etc.*) = = 2.24 Å, P_3—P_4 = 2.01 Å, and Rh—P_1 = 2.74 Å. The H_3P—Rh—PH_3 angle was computed to be 175°. Most importantly the optimized energy for the η^2 geometry is now 15 kcal/mol *more stable* than the optimized η^1 structure. Here Θ (defined in **15**) was 102°. The agreement with the experimentally determined structure[7] of **2** is marginal. The P_2—P_3 (*etc.*) bond lengths average to 2.21 Å. The P_3—P_4 bond is slightly shortened (2.19 Å) but not as much as in our optimized structure. The Rh—P_1 distance (2.29 Å) was much shorter than we have calculated it to be. Finally, the P_1—P_2 distance was significantly longer than the other P—P distances, however, it is only 2.46 Å (Θ = 79.6°). Our calculations do show the expected features which maximize bonding of the metal to an edge of P_4. Namely, there is increased bonding between the filled $3a_1$ orbital of P_4 (see Figure 4) and empty $2a_1$ on Rh $(PH_3)_2Cl$. This is evident from a plot of the bonding molecular orbital, labeled a_1 in Figure 3. In Figure 5a, this orbital is shown at the undistorted T_d geometry for P_4. Most of the electron density remains in the P_4 region. Figure 5c shows that same molecular orbital at the optimized geometry. It is clear that the electron density is more evenly divided between both fragments and is concentrated in the Rh—P bonding region. Figures 5b and d illustrate the analogous trend for the filled molecular

orbital labeled $2b_2$ in Figure 3. There is again much more efficient Rh—P bonding at the optimized geometry in Figure 5d than that in Figure 5b. Our calculations overemphasize the distortion. This is particularly evident for the $2b_2$ molecular orbital. As Θ increases this molecular orbital is considerably stabilized and falls between the $1a_1 + b_1 + a_2$ metal-centered orbitals in Figure 3. With the increasing involvement of the χ_1 component of t_1 into the $2b_2$ molecular orbital (as Θ increases), the P_3—P_4 distance is expected to contract. As shown in Figure 1 this orbital is bonding between P_3 and P_4 in a π-type fashion. This is the reason behind why our calculations for the optimized structure predict that it should be so short. Notice also in Figure 4 that at $\Theta \sim 90°$ the $2b_2$ LUMO of P_4 lies lower in energy than the $1b_2$ fragment orbital of $Rh(PH_3)_2Cl$. Consequently a large amount of electron density is transfered from the metal to the P_4 unit. Going from the undistorted P_4 geometry to the observed x-ray structure to the optimized one the occupation of the χ_1 component in t_1 ($2b_2$) for the *complex* increases from 0.488 to 0.838 to 1.605 electrons, respectively. This is also reflected in the charges calculated for Rh which increase from + 0.396 to 0.713 to 1.294 along this series.

What we have been describing in electronic terms is the oxidative insertion of a 14 electron $Rh(PH_3)_2Cl$ unit into a P—P bond of the P_4 cluster. The resulting product can be formulated in **16** as a 16 electron trigonal bipyramid.

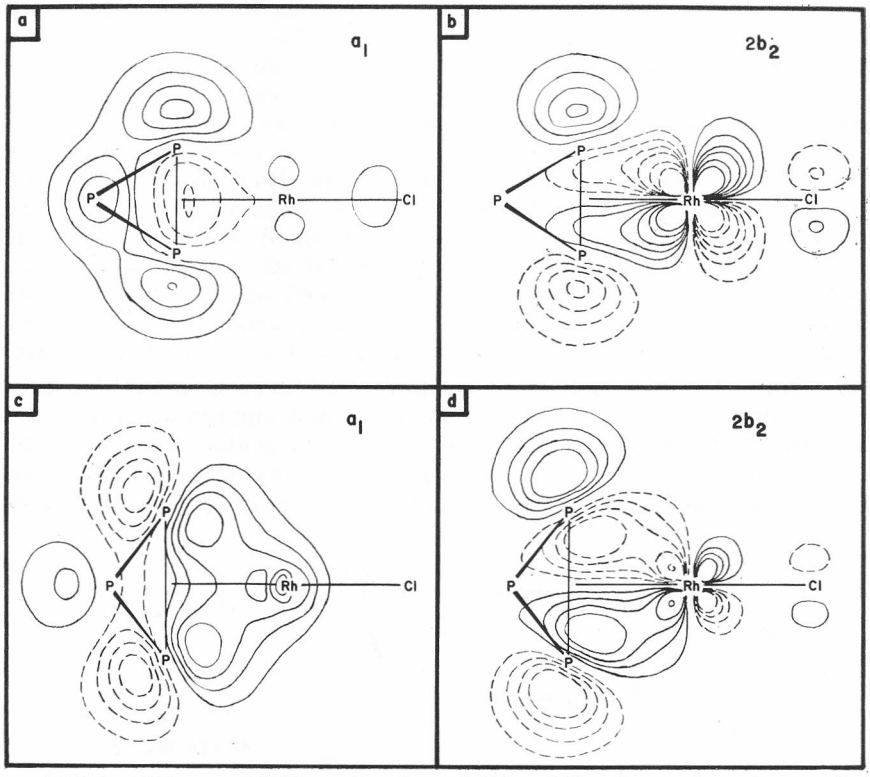

Figure 5. Plots of the a_1 and $2b_2$ molecular orbitals of the η^2 complex at an undistorted ($\Theta = 70.52°$) geometry in a and b and optimized ($\Theta = 102°$) structure in c and d. The contours have the values of 0.025, 0.05, 0.075, 0.10, 0.15, and 0.20. The dashed and full lines refer to opposite signs of Ψ.

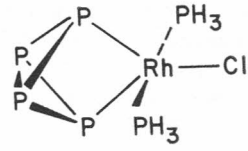

16

This reaction type does indeed have precedent. $IrCl(CO)(PPh_3)$ is inserted into the P_4S_3 cluster.[4f] In this case a dimeric compound with an octahedral, 18 electron coordination around each Ir atom is formed. Significantly the P—P distance of the cleaved bond is opened from 2.24 Å in the free ligand to 3.06 Å in the complex. This is close to the value that we find for the optimized η^2 complex of P_4. There is clearly not much bonding between P_1 and P_2 in our optimized structure. One way to quantify this in an approximate manner is *via* the Mulliken overlap population. In the free P_4 ligand the P_1—P_2 overlap population is 0.585. It is reduced slightly to 0.405 in the η^2 complex at a T_d geometry. At the experimentally determined structure it is much smaller (0.136) and at the optimized structure we find the overlap population to be negative (— 0.105) which is typical for nonbonded atoms. The situation here is not unlike that for the metal-olefin *versus* metallacyclopropane controversy.[10a,c] The two modes of bonding between ML_3 and P_4, namely forward donation of P_4 to ML_3 of a_1 symmetry and backdonation from ML_3 to P_4 of b_2 symmetry, are very close to the Dewar-Chatt-Duncanson model of metal-olefin bonding. It is difficult to determine, however, whether the compound is represented better as an η^2 complex to the P—P bond (as drawn at the top of Figure 3) or the oxidative insertion product **16**. $Rh(P_4)(PPh_3)_2Cl$ is perhaps closer to the η^2 formulation but our calculations at the experimental geometry do point to a substantial reduction of the P_1—P_2 bond order.[12] What we should realize is that there ought to be a continuum of structures that lie between these two extremes. The substitution of π-donors around the metal should raise the energy of the $1b_2$ fragment orbital making donation of electron density of χ_1 in t_2 more efficient. This will push the ground state structure towards **16**.

The careful reader will have realized that there is something peculiar about the formulation of especially **16** as a trigonal bipyramidal complex. This is a 16 electron compound, but the vast majority of pentacoordinate complexes have an 18 electron count. The normal splitting pattern for a D_{3h} trigonal bipyramid[13] is given in **17**. In a formal sense the χ_1 component of t_2 becomes

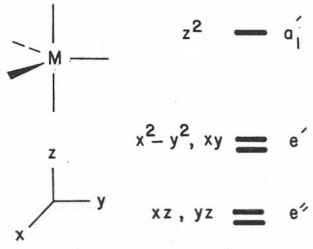

17

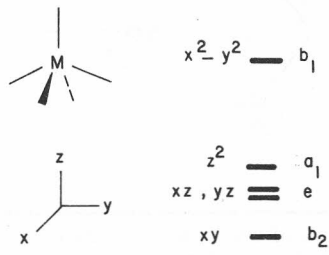

18

doubly occupied so the Rh is d^6. That will half-fill the e' set in **17** and a high spin complex is anticipated. One empty molecular orbital in the η^2 complex is appreciably stabilized as Θ is increased. It is labeled $3b_2$ in Figure 3 and its derivation is identical to the xy component of e' in **17**. However, it is energetically well-separated from the HOMO at the optimized structure. The reason behind this lies in the fact that the P_1—Rh—P_2 angle is only 69.5° at the optimized geometry. This is far away from the angle of 120° between two equatorial ligands in **17**. We shall not belabor the point here but this insures that the xy component of e' lies at a higher energy than the $x^2 - y^2$ component. Instead, we direct the reader to the analysis of distortions in six-coordinate complexes by Kubacek and Hoffmann[14] where identical considerations have been given for low electron count complexes. This point of view does easily show why the alternative η^2-isomer, **5**, is so much less stable than the others. First of all, the bite angle for even a widely opened P_4 ligand is quite small for a square pyramidal (**5**) molecule. Secondly, there is a very small HOMO--LUMO gap. The splitting pattern for a C_{4v} square pyramid is given in **18**. An orbital which is basically z^2 is the LUMO in our calculations of **5**. Any distortion of the P_4 ligand does not have an effect on z^2. Therefore, this geometry is not thought to be a viable one for complexes of P_4.

In conclusion, the η^1 (**3**) and η^2 (**4**) coordination modes of P_4 to a d^8-ML_3 unit can be made energetically quite close to one another when geometrical optimization of the P_4 ligand is taken into account. An η^1 coordination geometry will be favored when the $x^2 - y^2$ hybrid, $2a_1$ in Figure 2 lies low in energy, close to χ_3 of $2t_2$ and $2a_1$ on P_4. Weak σ-donor ligands around the metal will accomplish this task. A high-lying $1b_2$ orbital on the metal will favor interaction with the χ_1 component of t_2. Therefore, the substitution of a strong π donor *trans* to the P_4 ligand favors the η^2 mode of bonding.

η^1-Tetrahedral and η^3 Bonding

The orbitals of a pyramidal ML_3 species have been discussed extensively elsewhere.[10,15] Figure 6 presents an interaction diagram for a pyramidal, C_{3v}, ML_3 fragment interacting with P_4 at an η^1 geometry. On the right side of the Figure are displayed the valence orbitals of an arbitrary C_{3v} ML_3 fragment. At low energy are the three reminants of the octahedral t_{2g} set. They are labeled $1a_1$ and $1e$. At higher energy are three hybrid orbitals. The $2e$ set is primarily metal d with some p character mixed into them so they are hybridized away from the three auxiliary ligands, L, towards the P_4 unit. The $2a_1$ fragment orbital contains basically metal s and p character and is hybridized in the same direction as the $2e$ set. The χ_3 component of $2t_2$ and the $2a_1$ orbital of P_4 (see the right side of Figure 1) are stabilized by $1a_1$ and $2a_1$ on ML_3. χ_2 and χ_3 on $2t_2$ and the e set of P_4 are left nonbonding. Likewise, the $1e$ set on ML_3 will overlap with P_4 in primarily a δ type fashion and so it remains nonbonding. The $1a_1$ fragment orbital on ML_3 is destabilized by χ_3 of $2t_2$ and $2a_1$ from P_4. What stops it from rising to excessively high energies is that the $2a_1$ fragment orbital on ML_3 mixes into this molecular orbital in a way which is bonding to χ_3 components of t_1 on the P_4 fragment. These two molecular orbitals along with that previously described for $1a_1$ on ML_3 are very close to being degenerate. Therefore, the classic splitting pattern of three above two for a tetrahedral complex is established. A low spin d^8 complex (like $Rh(PH_3)_2Cl$) will

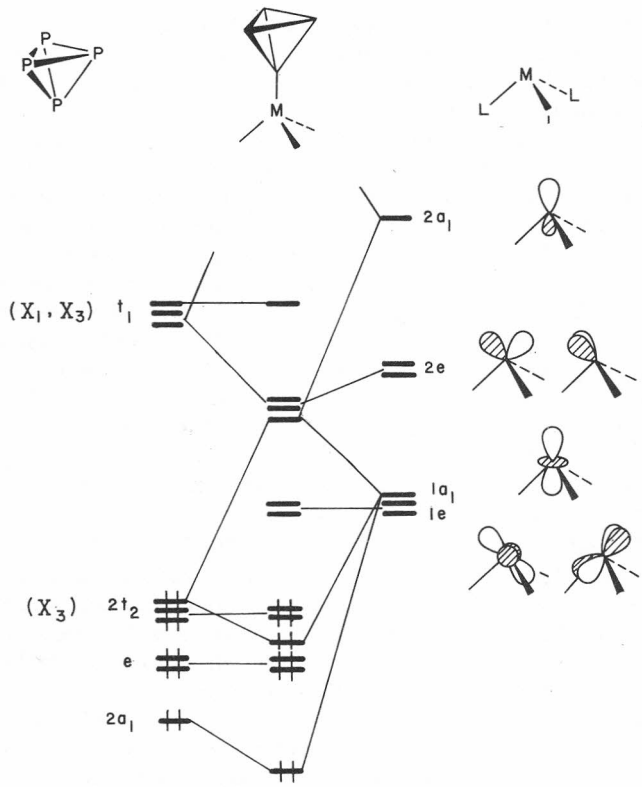

Figure 6. An interaction diagram for an η^1-tetrahedral-ML_3 complex.

not be stable at this geometry. The three molecular orbitals of the triply »degenerate« set will be occupied by only four electrons. A first order Jahn--Teller distortion relaxes the ML_3 unit back to a square planar structure, thus **6** does not represent a minimium on the potential energy surface. With two additional electrons (*i. e.* a d^{10} complex) these three molecular orbitals are totally occupied. As mentioned in the Introduction there exists one example of this type. The structure of **1** is quite close to what one expects for a tetrahedral complex. Notice in Figure 6 that with the 2*e* set formally filled in such a d^{10} complex there is appreciable backbonding to the χ_1 and χ_3 components of t_1 on P_4. This backbonding should be reflected in a shorted M—P distance and, since χ_1 and χ_3 of t_1 are antibonding between the coordinated phosphorus atom and the other three, these three P—P distances should be longer than the other three »basal« P—P bond lengths. This is found in **1**.[5] The Ni—P distance is ~ 0.2 Å shorter than normal. The distances of the coordinated phosphorus atom to the other three are 2.20 Å while the three basal P—P distances are 2.09 Å.

No categorized complex of the η^3 type exists. Much of the strategy for stabilizing this coordination mode can be extrapolated from the η^3—P_3—ML_n system.[2a,3] There is, however, one interesting twist that the P_4 ligand presents. An obvious candidate for stabilizing an η^3—P_4 ligand is the pyramidal, C_{3v}, ML_3 fragment. A simplified interaction diagram is shown in Figure 7. The χ_3

component of $2t_2$ and $2a_1$ on P_4 are stabilized somewhat by the $2a_1$ orbital on ML_3. Using a normal coordinate system where the z axis is coincident with the three-fold rotation axis of ML_3, the $1a_1$ along with $1e$ in ML_3 remain nonbonding. The $2e$ set of ML_3 overlaps to an approximately equal extent with χ_1 and χ_3 of t_1 and e. The overlap of $2e$ to the χ_1 and χ_2 components of $2t_2$ is much smaller. The resultant molecular orbital diagram in Figure 7 follows the typical splitting pattern of an octahedral complex with three metal centered orbitals below two, *i. e.* t_{2g} below e_g. A d^6 complex should be stable. Our calculations on a $Rh(PH_3)_2Cl^{2+}$ complex yield a binding energy of the ML_3 fragment to P_4 that is somewhat on the small side (13 kcal/mol), however, not much reliance should be put on this result since we have not optimized the geometry. What is somewhat worrisome is that the »e_g« set is at relatively low energy because of the overlap of $2e$ on ML_3 to χ_1 and χ_3 in t_1. Consequently a rather small energy gap (1.1 eV) between the HOMO and LUMO is found. Thus, while a d^6 complex of, for example, $Cr(CO)_3$ may be isolated, it ought to be quite reactive.

Referring back to Figure 7, one can see that there is a large energy gap between the $2e$ set on ML_3 and e of P_4. If this can be made smaller, then more favorable bonding will result between P_4 and the ML_n fragments. An ML_n fragment which encorporates this feature is the C_{3v} ML_4 one. The valence

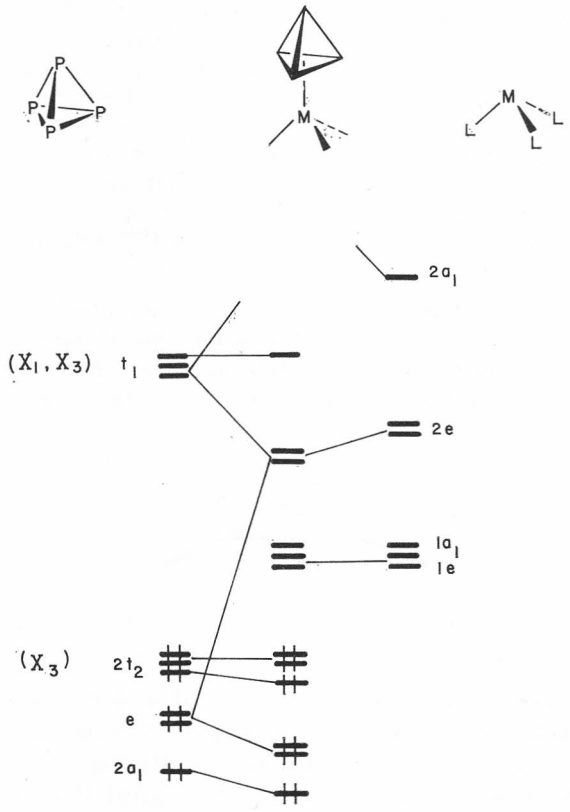

Figure 7. An orbital interaction diagram for an η^3—P_4—ML_3 complex.

orbitals of this fragment[10] are shown in **19**. The 1*e* set is basically *xz* and *yz* using the coordinate system in **19**. It lies at much lower energy than the 2*e* set in ML_3. Consequently it will stabilize the *e* set on P_4 to a greater extent. The

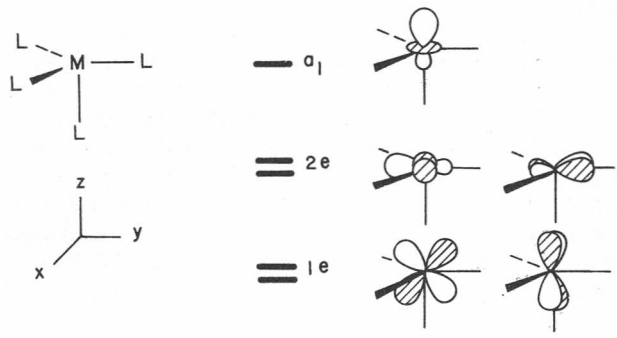

19

2*e* set of ML_4 because of its δ symmetry will not overlap to a significant extent with the orbitals of P_4. Therefore, the antibonding combination of 1*e* with the *e* set on P_4 should lie at a higher energy than the 2*e* set of ML_4. A d^4 complex is then expected to be stable. We do find this basic pattern on a model calculation of $P_4Fe(CO)_4^{4+}$. However, we hasten to add that there are severe steric constraints at work here. With a Fe—P distance of 2.30 Å and P—P distances of 2.21 Å, the equatorial carbonyl groups are quite close to the basal phosphorus atoms (2.48 Å). Thus, nonbonded repulsions between the filled CO π orbitals and filled orbitals on P_4 dominate and we find that the two fragments are not bound. One could bend the equatorial carbonyl groups away from the P_4 unit, however, this will serve to rehybridize the 1*e* set[10b] with a concomitant loss of overlap to the *e* set on P_4.

The best candidate that we have found for an η^3—P_4 complex is not a mononuclear one, but a trinuclear transition metal species. An $Fe_3(CO)_9$ fragment[16] has three empty valence orbitals, as shown in **20**, which are directed towards cluster. They are individually equivalent to the a_1 orbital in **19**. Linear

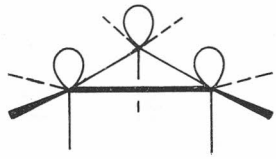

20

combinations of these three generate orbitals of $a_1 + e$ symmetry. They now match the symmetry properties and overlap well with the three members of the $2t_2$ set of P_4. A substantial HOMO-LUMO gap and healthy overlap population (0.826) between the two fragments suggest that this complex may be a viable possiblity. We look forward to experimental tests in this direction.

Acknowledgments. — We thank Professors Ted Lindsell, Alan Welch, and Roald Hoffmann for communications and preprints of their work. We also thank the Robert A. Welch Foundation for support and S.-H. Kang for skillful rendering of the drawing.

APPENDIX

All calculations were performed using the extended Hückel method[17] using the modified Wolfsberg-Helmholz technique.[18] The H_{ii}'s for Rh were obtained from a charge iteration on $P_4Rh(PH_3)_2Cl$ at an η^1 geometry using a T_d symmetry for P_4. The orbital exponents for Rh were taken from Basch and Gray.[19] The other parameters were taken from previous work.[15] The values of the H_{ii}'s and orbital exponents are listed in Table I. The Rh—Cl, Rh—$P(H_3)$, and P—H distances used were 2.34, 2.30, and 1.41 Å, respectively. All calculations employed H—P—H angles of 90°. The Fe—C, C—O, and Fe—Fe distances used were 1.78, 1.14, and 2.53 Å, respectively. In $P_4Fe_3(CO)_9$ the Fe—P distance were 2.41 Å.

TABLE I

Parameters Used in the Extended Hückel Calculations

Orbital	H_{ii}/eV	ζ_1	ζ_2	C_1[a]	C_2[a]
Rh	4*d* —10.51	4.29	1.97	0.5807	0.5685
	5*s* —6.63	2.135			
	5*p* —3.39	2.10			
Fe	3*d* —12.70	5.35	1.801	0.5366	0.6678
	4*s* —9.17	1.90			
	4*p* —5.37	1.90			
P	3*s* —18.60	1.60			
	3*p* —14.00	1.60			
Cl	3*s* —30.00	2.033			
	3*p* —15.00	2.033			
C	2*s* —21.40	1.625			
	2*p* —11.40	1.625			
O	2*s* —32.30	2.275			
	2*p* —14.80	2.275			
H	1*s* —13.60	1.30			

[a] Contraction coefficients used in the double zeta expansion.

REFERENCES

1. (a) Camille and Henry Dreyfus Teacher-Scholar, 1979—1984. Alfred P. Sloan Research Fellow, 1982—1984; (b) Present address, Department of Chemistry, Cornell University, Ithaca, NY 14853.
2. (a) For a review see M. Di Vaira and L. Sacconi, *Angew. Chem.* **94** (1982) 338; *Angew. Chem. Int. Ed. Engl.* **21** (1982) 330; (b) P. Dapporto, L. Sacconi, P. Stoppioni, and F. Zanobini, *Inorg. Chem.* **20** (1981) 3834; (c) M. Di Vaira, L. Sacconi, and P. Stoppioni, *J. Organomet. Chem.* **250** (1983) 183; (d) M. Di Vaira, M. Peruzzini, and P. Stoppioni, *Acta Crystallogr. Sect. C* **39** (1983) 1210; (e) M. Di Vaira, G. A. Ghilardi, S. Midollini, and Sacconi, *J. Amer. Chem. Soc.* **100** (1978) 2550; (f) M. D. Vaira, S. Midollini, and L. Sacconi, *ibid.* **101** (1979) 1757; (g) C. Bianchini, M. Di Vaira, A. Meli, and L. Sacconi, *ibid* **103** (1981) 1448; (h) F. Cecconi, P. Dapporto, S. Midollini, and L. Sacconi, *Inorg. Chem.* **17** (1978) 3292; (i) C. A. Ghilardi, S. Midollini, A. Orlandini, and L. Sacconi, *ibid* **19** (1980) 301; (j) C. Bianchini, M. Di Vaira, A. Meli, and L. Sacconi, *ibid* **20** (1981) 1169; (k) C. Bian-

chini, C. Mealli, A. Meli, and L. Sacconi, *Inorg. Chim. Acta* **37** (1979) L543.
3. For theoretical calculations see Ref. 2a and S. Shen-shu and R. Hoffmann, submitted for publication.
4. (a) G. Schmid and H. P. Kempry, *Z. Anorg. Allg. Chem.* **432** (1977) 160; (b) A. Vizi-Orotz, *J. Organomet. Chem.* **111** (1976) 61; (c) G. Fritz and R. Uhlmann, *Z. Anorg. Allg. Chem.* **465** (1980) 51; (d) W. Hönle and H. G. Von Schnering, *ibid* **465** (1980) 72; (e) A. W. Cordes, R. D. Joyner, R. D. Shores, and E. D. Dill, *Inorg. Chem.* **13** (1974) 32; (f) C. A. Ghilardi, S. Midollini, A. Orlandini, *Angew. Chem.* **95** (1983) 801; *Angew. Chem. Int. Ed. Engl.* **22** (1983) 790; (g) For theoretical computations on several P_n clusters see R. Gleiter, M. C. Böhm, M. Eckert-Maksić, W. Schäfer, M. Baudler, Y. Aktalay, G. Fritz, and K.-D. Hoppe, *Chem. Ber.* **116** (1983) 2972; R. Gleiter, M. C. Böhm, and M. Baudler, *ibid* **114** (1981) 1004; M. C. Böhm and R. Gleiter, *Z. Naturforsch. Teil B* **36** (1981) 498; W. W. Schoeller and T. Dabisch, *J. Chem. Soc., Dalton Trans.* (1983) 2411; W. W. Schoeller and C. Lerch, *Inorg. Chem.* **22** (1983) 2992.
5. P. Dapporto, S. Midollini, and L. Sacconi, *Angew. Chem.* **91** (1979) 510, *Angew. Chem. Int. Ed. Engl.* **18** (1979) 469.
6. (a) W. E. Lindsell, *J. Chem. Soc. Chem. Commun.* (1982) 1422; (b) A. P. Ginsberg, W. E. Lindsell, and W. E. Silverthorn, *Trans. N. Y. Acad. Sci.* **33** (1971) 303; (c) A. P. Ginsberg and W. E. Lindsell, *J. Amer. Chem. Soc.* **93** (1971) 2082.
7. W. E. Lindselll, K. J. McCullough, and A. J. Welch, *ibid* **105** (1983) 4487.
8. L. E. Sutton, *Chem. Soc. Spec. Pub.* No. **11** (1958).
9. (a) R. R. Hart, M. B. Robin, and N. A. Kuebler, *J. Chem. Phys.* **42** (1965) 3631; C. R. Brundle, N. A. Kuebler, M. B. Robin, and H. Basch, *Inorg. Chem.* **11** (1972) 20; (b) S. F. A. Kettle, *Theor. Chim. Acta* **4** (1966) 150; (c) R. M. Archibald and P. G. Perkins, *Chem. Commun.* (1970) 569; (d) M. F. Guest, I. H. Hillier, and V. R. Saunders, *J. Chem. Soc. Faraday Trans. 2* **68** (1972) 2070; (e) R. Osman, P. Coffey, and J. R. van Wazer, *Inorg. Chem.* **15** (1976) 287.
10. (a) T. A. Albright, R. Hoffmann, J. C. Thibeault, and D. L. Thorn, *J. Amer. Chem. Soc.* **101** (1979) 3801; (b) M. Elian and R. Hoffmann, *Inorg. Chem.* **14** (1974) 1058; (c) T. A. Albright, *Tetrahedron* **38** (1982) 1339; (d) *Molecular Shapes,* J. K. Burdett, New York, Wiley-Interscience, 1980, pp. 219—231.
11. For example, the overlap between $2a_1$ on ML_3 with χ_3 in the $2t_2$ set was 0.0196 while the between $2a_1$ and χ_2 of the set was 0.3004.
12. At this geometry the P_4 unit is computed to be bound to the $Rh(PH_3)_2Cl$ unit, however, it is still 25 kcal/mol higher in energy than the optimized η^1 structure.
13. A. R. Rossi and R. Hoffmann, *Inorg. Chem.* **14** (1975) 365.
14. P. Kubacek and R. Hoffmann, *J. Amer. Chem. Soc.* **103** (1981) 4320.
15. T. A. Albright, P. Hofmann, and R. Hoffmann, *ibid* **99** (1977) 7546.
16. B. E. R. Schilling and R. Hoffmann, *ibid* **101** (1979) 3456.
17. R. Hoffmann, *J. Chem. Phys.* **39** (1963) 1397; R. Hoffmann and W. N. Lipscomb, *ibid* **36** (1962) 2179; **37** (1962) 2872.
18. J. H. Ammeter, H.-B. Bürgi, J. C. Thibeault, and R. Hoffmann, *J. Amer. Chem. Soc.* **100** (1978) 3686.
19. H. Basch and H. B. Gray, *Theor. Chim. Acta* **4** (1966) 367.

SAŽETAK

Vezanje P_4 na d^8 — ML_3 kompleksima

Sung-Kwon Kang, Thomas A. Albright i Jerome Silvestre

Razmatrani su η^1, η^2 i η^3 kompleksi P_4-grozda s $Rh(PH_3)_2Cl$ primjenom proširene Hückelove (EH) metode. Najstabilnije su strukture η^1-kvadratni i η^2-kompleks C_{2v}-simetrije; d^{10} — η^1 tetraedarski kompleks također je prilično stabilan. Najboiji kandidat za tip vezanja η^3 jest trimer $Fe_3(CO)_9$.

CROATICA CHEMICA ACTA CCACAA 57 (6) 1371—1386 (1984)

YU ISSN 0011-1643
CCA-1528 UDC 541
Original Scientific Paper

Interaction of the Hydrogen Molecule with the Palladium Atom. A Force Theoretic Study

Hiroshi Nakatsuji and Masahiko Hada

Division of Molecular Engineering, Graduate School of Engineering, Kyoto University, Kyoto 606, Japan

Received February 3, 1984

As a model of chemisorption, we studied an interaction of the H_2 molecule with the $^1S(4d^{10})$ and $^3D(4d^95s^1)$ states of the Pd atom. We calculated an accurate Hellmann-Feynman force acting on the H_2 molecule by adding the first derivatives of the hydrogen basis set. The force and density origins of the interaction were clarified. The singlet Pd(^1S) — H_2 system, which is the ground state, is attractive but the triplet Pd(^3D) — H_2 system is repulsive. The side-on approach is a preferable path. For the Pd(^1S) — H_2 system, the Pd—H bonds are gradually formed. The electron density is accumulated in the overlap region of the H_2 molecule and the Pd atom and it pulls the H_2 molecule onto the Pd atom. The bond of the H_2 molecule is gradually weakened. The electrons are transferred from the bonding MO of the H_2 molecule to the empty 5*s* and $5p_z$ AO's of the Pd atom. For the Pd(^3D) — H_2 system, the density of the Pd atom tends to keep its spherical symmetry even when the H_2 molecule approaches. The Pd atom in the $4d^95s^1$ configuration is more repulsive than that in the $4d^{10}$ configuration. Therefore, the H_2 molecule is repelled by the Pd atom.

I. INTRODUCTION

Chemisorption of hydrogen molecules on transition metals is an important step for hydrogen storage and activation of molecular hydrogen followed by a variety of catalytic processes.[1–4] Palladium shows, especially, a unique affinity for hydrogen. The »solubility« of hydrogen in palladium metal markedly exceeds that in the other group 8 metals.[1] Molecular hydrogen can diffuse through metallic palladium at a higher rate than in other platinum-series metals. This process is very selective so that it is used for the purification of hydrogen gas from a mixture. Further, homogeneous palladium complexes also show a variety of catalytic reactions including some industrially important ones (*e. g.*, Hoechst-Wacker reaction).[2–4]

The electronic structure and the bonding nature in the diatomics, PdH and PtH have been studied theoretically at various levels of approximation.[5–8] For these diatomic hydrides, bonding properties such as bond energy, force constant, *etc.*, are known experimentally for some lower electronic states[9], so that they offer a good test for various levels of theoretical method. Further, these metal hydrides are thought to be a model product of the dissociative chemisorption of the hydrogen molecule on the metal surface.

Bagus and Björkman[6] studied the bonding in NiH and PdH by an *ab initio* SCF and CI methods. The bonding between Pd and H is primarily due to the 5*s* electron in the metal. The *d*-electrons are localized on the metal and participate only slightly in the Pd—H bond. Pacchioni *et al.*[7] reported a multi--reference CI study on the PdH, PdC, and PdCO molecules based on the effective-core potential SCF MO's. They reported the importance of the choice of the Pd basis set and also of the effects of electron correlation. Their results showed that the effect of electron correlation on PdH is to deepen the potential energy curve. The equilibrium bond length and force constant calculated by the SCF method compare relatively well with experimental results, although for the dissociation energy the SCF result is only half of the experimental value. Wang and Pitzer[8] also reported a similar effect of electron correlation on PtH. The correlation energy has little effect on the bond length and force constant of the ground state of PtH, but it does contribute significantly to the binding energy. Basch and Topiol[5] and Wang and Pitzer[8] further pointed out the importance of the relativistic effect on the electronic structure of PtH.

Bagatur'yants *et al.*[10] studied the approach of the hydrogen molecule to the Pd atom with a fixed H—H length (0.74 Å). They carried out all electron SCF calculations with the minimal and extended basis sets. They showed that formation of the molecular complex is favorable energetically and analyzed the donor-acceptor interactions between H_2 and Pd. They pointed out the important role of the outer 5*s* and 5*p* AO's of the Pd atom in the formation of the Pd—H_2 complex.

In this paper we study the interaction of the H_2 molecule with the Pd atom, as a model of the electronic processes in the chemisorption of the hydrogen molecule. We use the effective-core potential (ECP) SCF method[11] for the Pd atom.[12] We include the relativistic effects through the ECP potential but neglect, in this paper, the effect of electron correlation. For the ground state of PdH and PtH, the effect of electron correlation was to deepen the potential minima without much affecting the equilibrium length and the force constant.[7,8]

The force concept based on the Hellmann-Feynman theorem gives a simple and intuitive method of studying chemical phenomena.[13,14] The force acting on the nucleus A, F_A is determined by the electrostatic interaction of the nucleus A with the electron cloud and the other nuclei surrounding it.

$$F_A = Z_A \int r_{A1}/r_{A1}^3 \, \varrho\,(r_1)\, dr_1 - Z_A \sum_{B(\neq A)} Z_B R_{AB}/R_{AB}^3 \qquad (1)$$

We used the force concept to obtain a deeper understanding of the nature of the interaction.

Further, an accurate and reliable calculation of the Hellmann-Feynman force has been realized recently.[15,16] It was shown that the Hellmann-Feynman theorem is essentially satisfied when we add the first derivative bases to the basis set conventionally used. The method has been applied to studies of molecular structure, molecular vibration and chemical reaction.[15-17] In the present model system of chemisorption, Pd—H_2, we are primarily interested in the force acting on the adsorbed molecule H_2, and not in the force acting on the metal, since the metal atom represents here a surface atom of the metal catalyst. Therefore, we have added the first derivatives only to the H_2 basis set which is the [2*s*] set of Dunning.[18] The added derivative bases describe

well the polarization of the H_2 electron cloud and lead to the satisfaction of the Hellmann-Feynman theorem for the force acting on the protons of the H_2 molecule. Wang *et al.*[8] found for PtH that the polarization functions centered on the H atom are more important than those centered on the Pt atom.

II. INTERACTION OF THE H_2 MOLECULE WITH THE Pd ATOM IN THE ^1S AND ^3D STATES

The ground state of the Pd atom is the closed-shell ^1S state with the configuration $4d^{10}$. The first excited state is the ^3D state with the configuration $4d^95s^1$. It lies 19 kcal/mol above the ground state. We have approached the H_2 molecule onto the Pd atom keeping the C_{2v} symmetry (side-on), because, as will be shown below, this is a favorable approach. The H—H length was kept fixed to 0.74144 Å and 1.0 Å. The former is the equilibrium distance of the free hydrogen molecule.

In Figure 1, we have shown the potential energy curves for the side-on approach of the H_2 molecule to the Pd atom. The figure on the left hand side corresponds to the fixed H—H distance of 0.74144 Å and the one on the right hand side corresponds to the H—H distance of 1.0 Å. The lower curve was obtained from the interaction of the singlet $4d^{10}$ state of the Pd atom with the H_2 molecule, and the upper curve was obtained from the interaction of the triplet $4d^95s^1$ state of the Pd atom with the H_2 molecule. Figure 1 shows that the singlet Pd (^1S)—H_2 system is attractive but the triplet Pd (^3D)—H_2 system is repulsive. The energy difference of the ^1S and ^3D states of the Pd atom was taken from the experimental value (19 kcal/mol). The calculated value for the atom was — 3 kcal/mol, (*i. e.*, the ^3D state was calculated to be lower than the ^1S state) because of the lack of electron correlation. The correlation energy is larger for the closed-shell singlet state than for the open-shell triplet state.

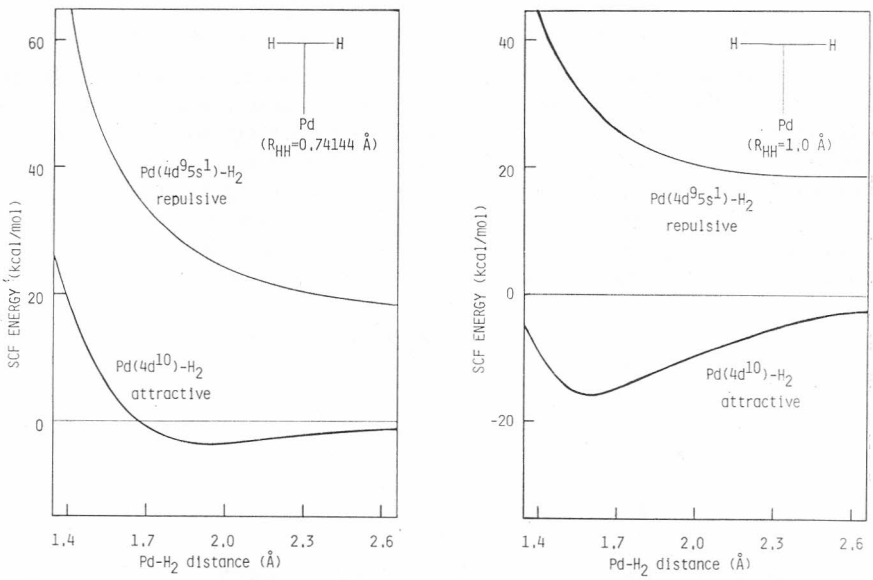

Figure 1. Potential energy curves for the interactions of the H_2 molecule with the ^1S ($4d^{10}$) and ^3D ($4d^95s^1$) states of the Pd atom. The figures on the left and right hand sides are for the fixed H_2 distances of 0.74144 Å (equilibrium length) and 1.0 Å, respectively.

The existence of the repulsive curve, not far from the attractive curve, is very interesting. It may work in the detachment process of the hydrogen molecule from the Pd metal.

When the H—H length is kept fixed at 0.74144 Å, the stabilization energy for the Pd (^1S)—H_2 system was calculated to be 3.6 kcal/mol. It is small in comparison with the experimental value, 9.6 kcal/mol, which is the heat of adsorption of the hydrogen molecule on the bulk palladium metal.[1] The stable Pd—H_2 distance was calculated at 1.90 Å. When the H—H length is elongated to 1.0 Å, the stabilization energy relative to the Pd atom and the elongated H_2 molecule becomes 15.9 kcal/mol and the stable Pd—H_2 distance becomes 1.62 Å, though 20.2 kcal/mol is necessary for this elongation of the free hydrogen molecule.

During the course of the approach, the H_2 molecule fixed at the equilibrium length, 0.74144 Å, receives the force, as shown below, which works to elongate the H—H distance. Therefore, in an actual process, the H_2 molecule approaches the Pd atom while gradually elongating its H—H distance. For this optimal approach the stabilization energy would become larger than the present value. However, in order to obtain a value comparable to the experimental value, inclusion of the electron correlation effect would be necessary. The roles of the second, third, ... Pd atoms of the metal surface are also of interest.

The triplet interaction of the Pd (^3D) atom and the H_2 molecule is repulsive, independent of the H—H distance, though the slope becomes smaller for the interaction with the elongated H_2. We will show later in the force theoretic analysis that the Pd atom in the $4d^95s^1$ configuration is more repulsive than that in the $4d^{10}$ configuration.

III. FORCE AND DENSITY ORIGIN OF THE INTERACTION

As seen from Eq. (1), the Hellmann-Feynman force depends on the three dimensional distribution of the electron density and nuclei. In the present Pd—H_2 system, we have two distinct subsystems which are the Pd atom and the H_2 molecule. We therefore divide the electron density regionally into the one belonging to the Pd atom, the one belonging to the H_2 molecule, and the one belonging to the overlap region of the Pd atom and the H_2 molecule. This regional partitioning of the electron density naturally leads to the analysis of the force acting on the proton of the hydrogen molecule as

$$F = \sum_{r}^{\text{on Pd}} \sum_{s} P_{rs} \langle r \,|\, f_{\mathrm{H}} \,|\, s \rangle - Z_{\mathrm{H}} Z_{\mathrm{Pd}} R_{\mathrm{H-Pd}} / R^3_{\mathrm{H-H}} \quad ; F(\mathrm{Pd})$$

$$+ \sum_{r}^{\text{on H}_2} \sum_{s} P_{rs} \langle r \,|\, f_{\mathrm{H}} \,|\, s \rangle - Z_{\mathrm{H}} Z_{\mathrm{H'}} R_{\mathrm{H-H'}} / R^3_{\mathrm{H-H'}} \quad ; F(\mathrm{H_2})$$

$$+ 2 \sum_{r}^{\text{onPd}} \sum_{s}^{\text{onH}_2} P_{rs} \langle r \,|\, f_{\mathrm{H}} \,|\, s \rangle \quad ; F(\mathrm{H_2—Pd}) \qquad (2)$$

where P_{rs} is the bond-order density matrix with respect to the bases r and s. The first term, F (Pd), represents the force acting on the proton due to the electrons and nucleus of the Pd atom, the second term, F (H_2) represents the force due to the electron density and the other proton of the H_2 molecule

adsorbed on the Pd atom, and the last term, F (H_2—Pd), represents the force due to the electron density accumulated in the overlap region of the AO's of the H_2 molecule and the Pd atom.

III A. *Preference of the Side-on Attack*

We first examine a preferable way of attack of the H_2 molecule on the Pd atom. We have put the H_2 molecule 2.0 Å apart from the Pd (^1S) atom and declined it by 10° from the C_{2v} side-on position. Table I shows the force

TABLE I

Force Acting on the H_a and H_b Atoms of the Hydrogen Molecule which is Side-on Slantwise on the Pd Atom. The H—H Distance is 0.74144 Å and the Distance Between Pd and the Center of H_2 is 2.0 Å

Term	H_a		H_b	
	$F_\perp$	$F_{//}$	$F_\perp$	$F_{//}$
F (Pd)	0.0210	0.0104	0.0301	0.0038
F (H_2)	—0.0046	0.0225	—0.0068	0.0203
F (H_2—Pd)	—0.0188	—0.0230	—0.0220	—0.0130
F (total)	—0.0024	0.0099	0.0013	0.0111

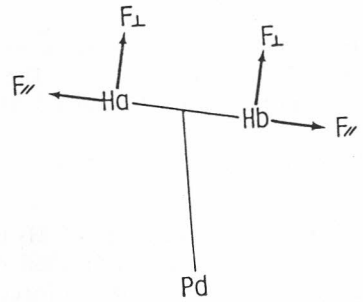

analysis and Figure 2 shows the contour map of the density difference defined by

$$\Delta\varrho = \varrho\,(\text{Pd—H}_2) - \varrho\,(\text{Pd}, {}^1S) - \varrho\,(\text{H}_2) \tag{3}$$

which shows the reorganization of the electron density due to the interaction between the Pd (^1S) atom and the H_2 molecule.

From the force perpendicular to the H—H axis, $F_\perp$, we see that the hydrogen molecule receive the force which acts to recover the C_{2v} approach. This recovery seems to occur with slipping down the H_2-rod onto the right-hand side, since the force paralell to the bond, $F_{||}$, is larger for H_b than for H_a. The H_2 molecule tends to elongate the bond as seen from the values of $F_{||}$.

The origin of the recovering force on the H_a atom, $F_{H_a\perp}$ is the sum of the forces F (H_2—Pd) and F (H_2), which overcomes the repulsion due to the Pd atom, F (Pd). As seen from Figure 2, the force F (H_2—Pd) reflects an increase in the electron density between the H_a and Pd atoms and F (H_2) reflects a polarization of the electron density near the H_a atom. The origin of the recovering force acting on H_b, $F_{H_b\perp}$, is the repulsion due to the Pd atom. Though

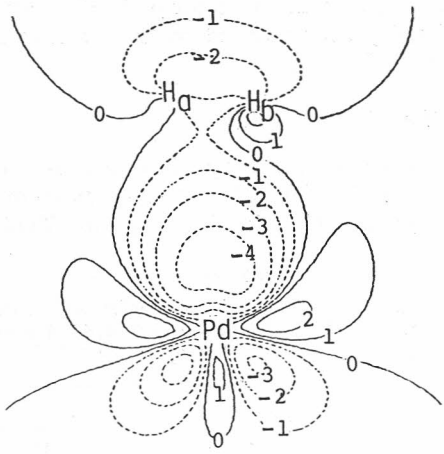

Figure 2. Density difference contour map for the singlet Pd (^1S)—H_2 system in which the H_2 molecule is side-on slantwise on the Pd atom. The H—H distance is 0.74144 Å and the distance between Pd and the center of H_2 is 2.0 Å. The definition of the density difference is given by Eq. (3). The real lines correspond to an increase in density and broken lines to a decrease, with the contour values of 0, ±1, ±2, ±3, ±4, and ±5 corresponding to 0.0, ±0.002, ±0.005, ±0.01, ±0.02, and ±0.05 a. u., respectively.

a polarization of the electron density near the H_b atom and a bonding interaction between the H_b and Pd atoms are seen from the density difference map, the extent is less than the repulsion due to the Pd atom.

III B. *Force and Density Origin of the Interaction for the Pd (^1S)—H_2 System*

We now consider the side-on approach of the H_2 molecule onto the Pd (^1S) atom. The force acting on the H_2 molecule is divided into the two components, F_z and F_y, shown in Figure 3. The negative of the force F_z is an attractive force of chemisorption, and the force F_y is the force which prolongs the H_2 molecule. Figure 4 shows the contour map of the density difference defined by Eq. (3) for several points of the side-on approach. The H—H distance was kept fixed at 0.74144 Å. In Figure 5, we have shown an analysis of the force of chemisorption, F_z, into the components defined by Eq. (2). The left and right hand sides correspond to the fixed H—H distances of 0.74144 Å and 1.0 Å, respectively. Figure 6 shows a similar analysis of the stretching force, F_y, along the adsorption process.

From the total force curve shown in Figure 5, we can estimate an equilibrium Pd—H_2 distance. It is 1.92 Å and 1.64 Å for the systems with the fixed H—H distances of 0.74144 Å and 1.0 Å, respectively. These results are in close agreement with those obtained from the potential energy curves shown in Figure 1 (1.90 Å and 1.62 Å, respectively). This is a matter of course since the present wavefunctions essentially satisfy the Hellmann-Feynman theorem.

From Figure 4, we can see a density origin of the 'chemisorption' of the H_2 molecule on the Pd (^1S) atom. As the H_2 molecule approaches, the Pd atom

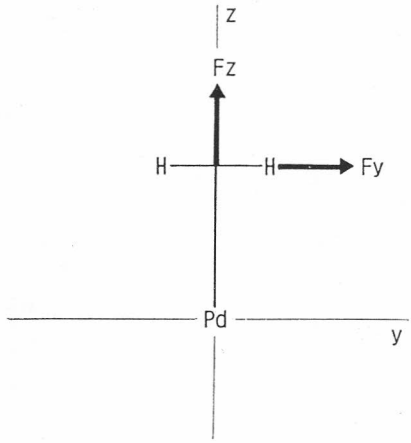

Figure 3. Definition of the force acting on the H_2 molecule which approaches side-on to the Pd atom.

extends its right and left lobes of the density from the outside of the H_2 molecule. These lobes grow up to form a bond between Pd and each hydrogen. It becomes conspicuous at 1.7 Å. From Figure 5, we confirm that the origin of the attractive force is the F (H_2—Pd) term. The electron density accumulated in the overlap region between H_2 and Pd attracts H_2 to chemisorb on the Pd atom. The Pd—H bonds are formed as the H_2 molecule approaches.

Further, as seen from Figure 4, the electron density decreases in the internuclear region of the H_2 molecule, so that the bond between the hydrogen atoms is weakened as the H_2 molecule approaches the Pd atom. As seen from Figure 6, the proton of the H_2 molecule always receive the force which prolongs the H_2 distance. The origin of this force is F (H_2). Namely, the decrease in the electron density in the H_2 molecule causes a deshielding of the inter-proton repulsion. The repulsion from the Pd atom, F (Pd), also works to elongate the H—H distance.

We will see later that the increase in the electron density in the overlap region of Pd and H_2 and the decrease in the density in the H_2 region are mainly due to an electron-transfer interaction from the bonding MO of the H_2 molecule to the vacant 5*s* and $5p_z$ AO's of the Pd atom.

When the H—H length is elongated, in response to the force shown in Figure 6, the electron density reorganizes itself as shown in Figure 7. It is for the H—H distance of 1.0 Å. The distance between Pd and H_2 is 2.0 Å. Comparing Figure 7 with the corresponding contour map shown in Figure 4, we see that an elongation of the H_2 distance very much facilitates the formation of the Pd—H bond. The left and right lobes of the Pd atom extend up to the two protons to form the Pd—H bond. In Figure 5, the effect of elongating the H—H distance on the force of interaction F_z is shown. The left and right figures correspond to the H—H distances of 0.74144 Å and 1.0 Å, respectively. By an increase in the H—H distance, the H_2 system receives more attractive force from the Pd atom. The origin is an increase in the F (H_2—Pd) force. Namely, the electron density more accumulated in the bond region of Pd and H as

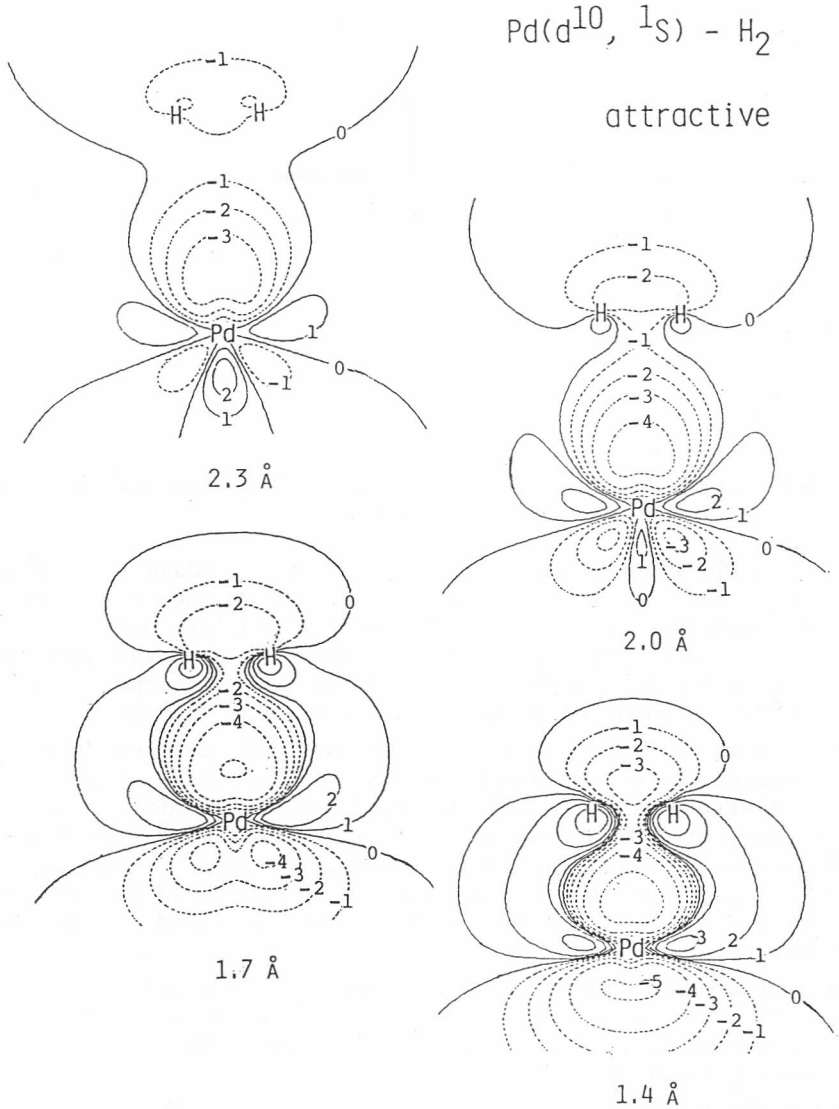

Figure 4. Density difference contour maps for the singlet Pd (d^{10}, ^1S)—H_2 system. The H—H distance is kept at 0.74144 Å and the distance between Pd and H_2 is given below each map. The definition of the density difference is given by Eq. (3). The real lines correspond to an increase in density and broken lines to a decrease, with the contour values of 0, ±1, ±2, ±3, ±4, and ±5 corresponding to 0.0, ±0.002, ±0.005, ±0.01, ±0.02, and ±0.05 a. u., respectively.

shown in Figure 7 attracts more the protons to the Pd atom. The other components of the force, F (H_2) and F (Pd), do not change much between the two systems.

The H_2 molecule receives the force F_y which prolongs the H—H distance when it is kept at 0.74144 Å. However, when it is elongated to 1.0 Å, the

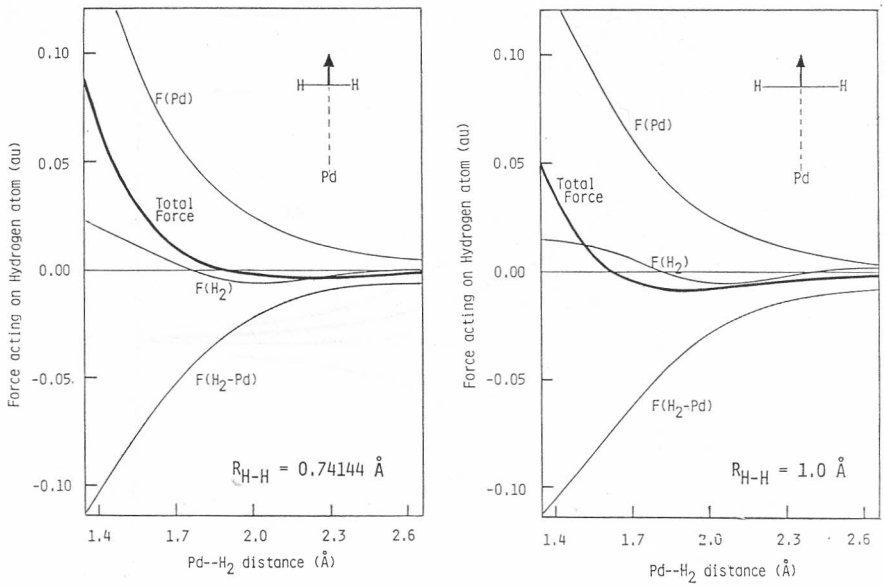

Figure 5. The analysis of the force F_z acting on the H_2 molecule of the singlet. Pd (^1S)—H_2 system. The definition of the forces is given by Eq. (2). The left and right hand sides correspond to the fixed H—H distances of 0.74144 Å and 1.0 Å, respectively.

protons receive the reverse force. At the Pd—H_2 separation of the 2.0 Å, the force F_y is 0.0037 a. u. for H_2 with $R_{HH} = 0.74144$ Å and —0.0828 a. u. for H_2 with $R_{HH} = 1.0$ Å. The equilibrium length of H_2 at this Pd—H_2 separation is estimated to be 0.772 Å.

The interaction between the H_2 molecule and the Pd atom may further be understood in terms of the electron transfer and back-transfer interactions as in the Dewar-Chatt-Duncanson model[20] of the interaction between platinum and the olefine double bond. In Figure 8, we have shown the population analysis of the Pd (^1S)—H_2 system along the Pd—H_2 distance. The upper side shows the changes in the gross atomic charges of the Pd and H atoms and the lower side shows the atomic orbital populations.

As the hydrogen molecule approaches the Pd atom, the electron is transferred from the H_2 molecule tc the Pd atom. Qualitatively speaking, the orbital interactions between the H_2 molecule and the Pd atom are that the bonding MO of H_2, σ_{H_2} donates an electron to the metal AO's and that the antibonding MO of H_2, $\sigma^*_{H_2}$ receives the back-donated electron from the Pd atom. The $4d_{z^2}$, $5s$, and $5p_z$ AO's of the Pd atom can interact with the bonding σ_{H_2} MO, and only the $4d_{yz}$ AO interacts with the antibonding $\sigma^*_{H_2}$ MO. In Figure 9, we have given an MO interaction diagram. As the H_2 molecule approaches, the $5s$, $5p_z$, and $4d_{z^2}$ AO's hybridize very rapidly and form $4d_{z^2} - (5s + 5p_z)$ hybrid and $(5s + 5p_z) + 4d_{z^2}$ hybrid with appropriate mixing coefficients (prehybridization step on the left hand side of Figure 9). The two electrons originally in the d_{z^2} AO occupy the former hybrid and the latter one is left unoccupied. The electron of the σ_{H_2} MO is transferred to the unoccupied hybrid and forms a bond

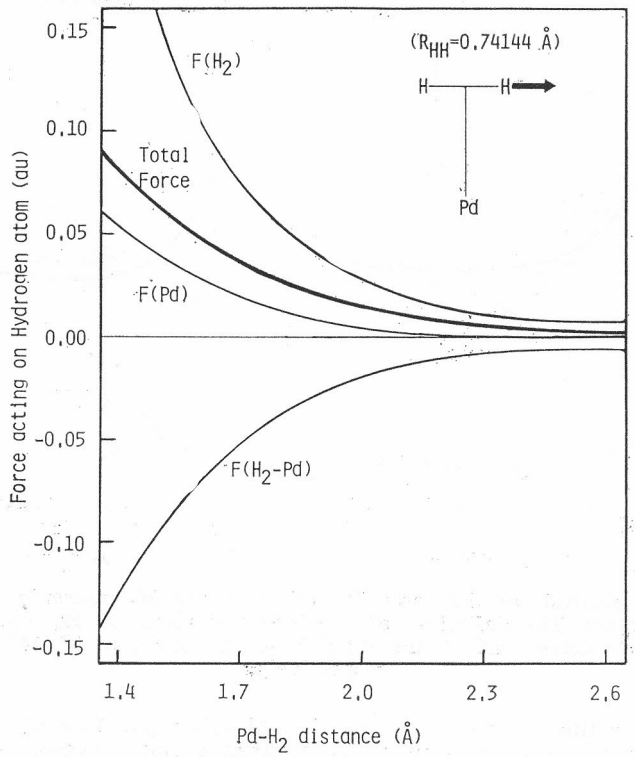

Figure 6. The analysis of the force F_y acting on the H_2 molecule of the singlet Pd (^1S)—H_2 system with the fixed H—H length of 1.0 Å. The definition of the forces is given by Eq. (2).

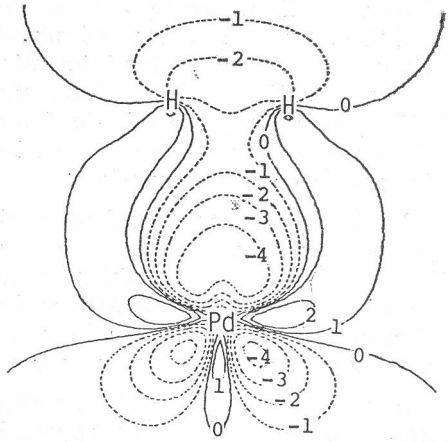

Figure 7. Density difference contour map for the singlet Pd (d^{10}, ^1S)—H_2 system with the H—H length of 1.0 Å and the Pd—H_2 distance of 2.0 Å. The density difference is defined by Eq. (3). The real lines correspond to an increase in density and broken lines to a decrease, with the contour values of 0, ±1, ±2, ±3, ±4, and ±5 corresponding to 0.0, ±0.002, ±0.005, ±0.01, ±0.02, and ±0.05 a. u., respectively.

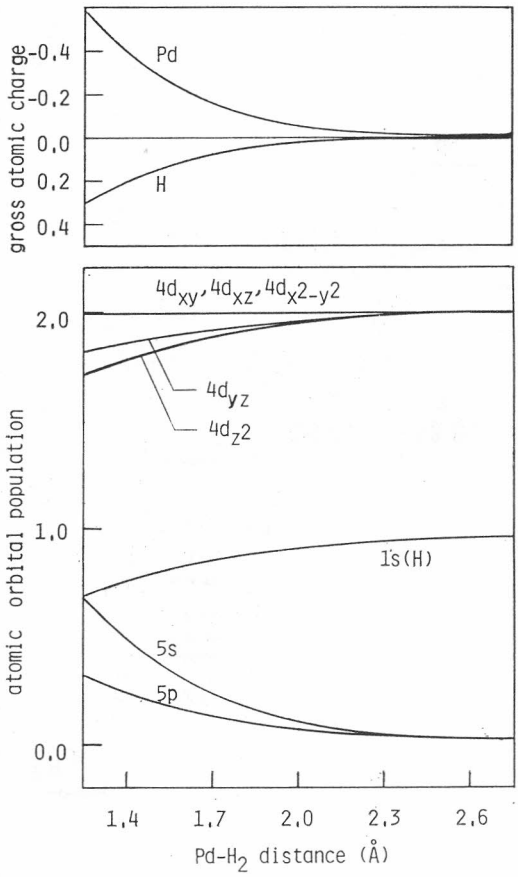

Figure 8. Gross atomic charge (upper side) and atomic orbital population (lower side) of the singlet Pd (^1S, $4d^{10}$)—H_2 system against the Pd—H_2 distance. The H—H distance was kept at 0.74144 Å throughout the approach.

between Pd and H_2. The increase in the $5s$ and $5p_z$ AO population and the decrease in the $4d_{z^2}$ AO population shown in Figure 8 are due to this MO interaction. The back-transfer interaction from the Pd $4d_{yz}$ AO to the $\sigma^*_{H_2}$ MO seems to be smaller than the transfer interaction.[10] The slope of the $4d_{yz}$ AO population is smaller than that of the $5s$ and $5p_z$ AO populations and the gross charge of the hydrogen atom is positive.

From the above discussion, we conclude that the bonding between the Pd atom and the H_2 molecule is primarily due to the overlap between the $5s$—$5p$ hybrid of the Pd atom and the $1s$ AO's of the H_2 molecule. The participations of the $4d$ AO's are secondary.

We note that the decrease in the electron density in the $4d_{z^2}$ AO is also understood as being due to the induced inner excitation of the electrons from the $4d_{z^2}$ AO to the $5s$ and $5p_z$ AO's caused by an interaction between Pd and H_2. Such an interaction is usually called the 'polarization' term.[21]

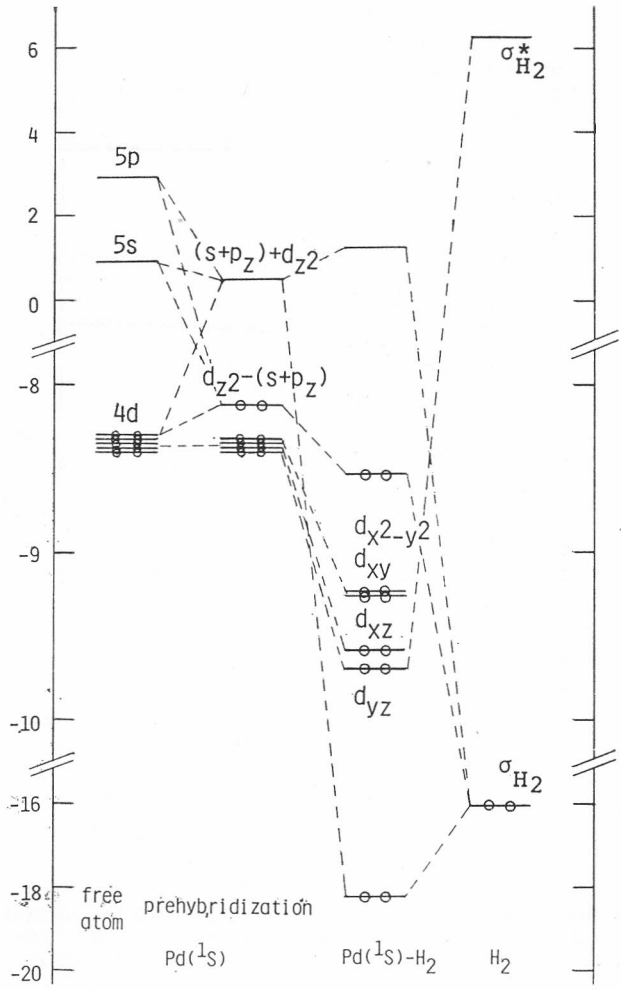

Figure 9. An MO interaction diagram for the singlet Pd (^1S, $4d^{10}$)—H_2 system.

III C. *Force and Density Origin of the Repulsive Interaction Between Pd (^3D) and H_2*

Though the singlet ground state of the palladium is attractive for H_2, the lowest triplet state is repulsive. Figure 10 shows the density difference map for the interaction between the H_2 molecule and the Pd atom in the ^3D (d^9s^1) state. It is defined by

$$\Delta\varrho = \varrho\,(\mathrm{Pd—H_2}) - \varrho\,(\mathrm{Pd}, {}^3D) - \varrho\,(\mathrm{H_2}) \tag{4}$$

where $\varrho\,(\mathrm{Pd}, {}^3D)$ is calculated for the averaged electronic configuration, $d_{xy}^2\, d_{zx}^2\, d_{yz}^{5/3}\, d_{z^2}^{5/3}\, d_{x^2-y^2}^{5/3}\, 4s^1$, which has circular symmetry on the yz plane. Figure 11 shows the force F_z and its analysis.

Even when the H_2 molecule approaches the Pd (^3D) atom up to 2.3—2.0 Å, the electron density does not accumulate well in the overlap region. At 2.0 Å,

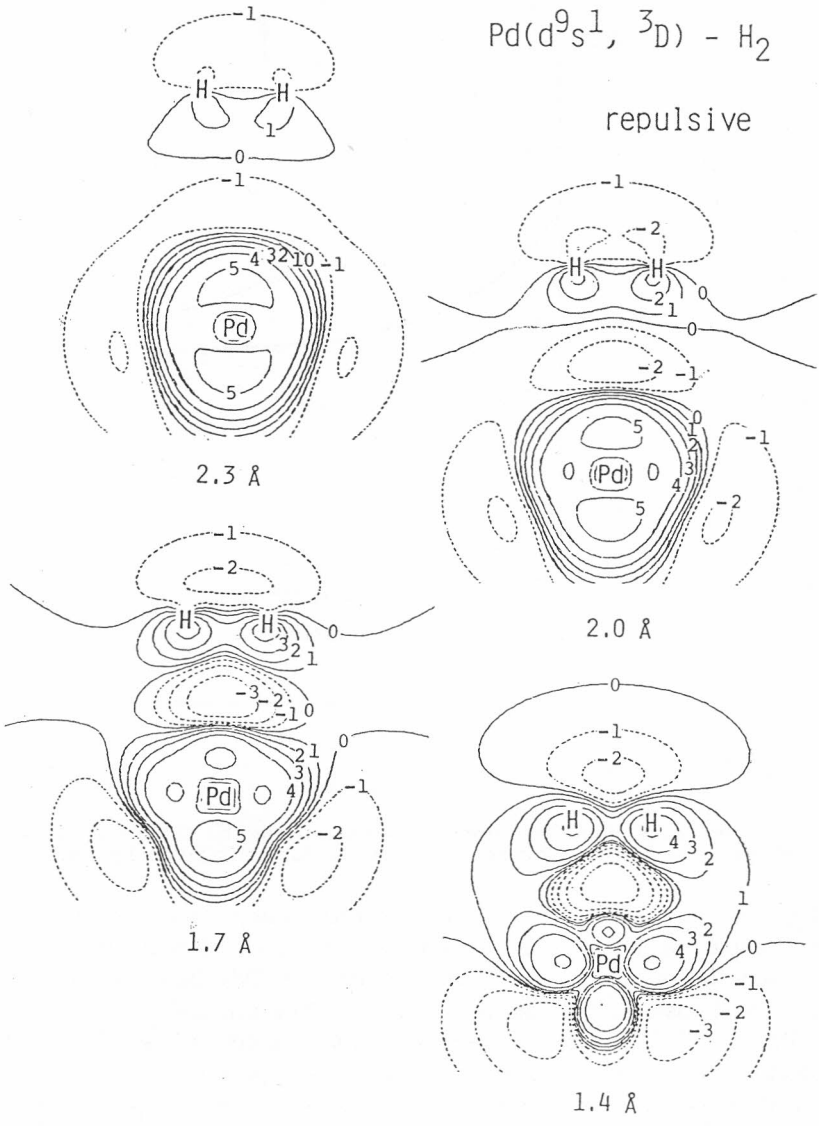

Figure 10. Density difference contour maps for the triplet Pd ($4d^9\,5s^1$, ^3D)—H_2 system. The H—H distance is kept at 0.74144 Å and the distance between Pd and H_2 is given below each map. The density difference is defined by Eq. (4). The real lines correspond to an increase in density and broken lines to a decrease, with the contour values of 0, ±1, ±2, ±3, ±4, and ±5 corresponding to 0.0, ±0.002, ±0.005, ±0.01, ±0.02, and ±0.05 a. u., respectively.

we find a line of 0.0 a. u. intersecting the Pd atom and the H_2 molecule. In comparison with the case of the attractive system, Pd (^1S)—H_2 shown in Figure 4, the electron density of the Pd atom shown in Figure 10 is less af-

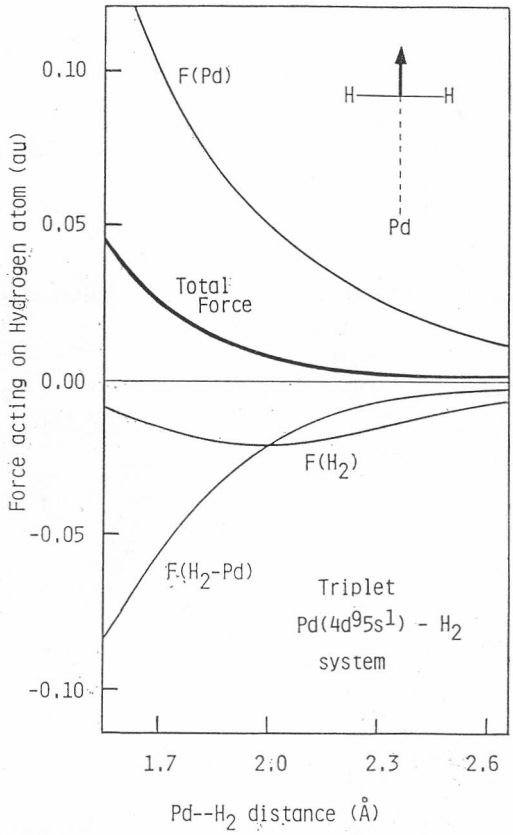

Figure 11. The analysis of the force F_z acting on the H_2 molecule of the triplet Pd (^3D)—H_2 system. The definition of the forces is given by Eq. (2).

fected by an approach of the H_2 molecule and tends to keep its spherical symmetry. Comparing the force analysis shown in Figure 11 with that of Figure 5, we see that the repulsion due to the Pd atom, F (Pd), increases more rapidly in the present case than in the previous case. The attractive part of the force, F (H_2—Pd) and F (H_2), can not overcome this repulsive force. The reason that the Pd atom in the $4d^95s^1$ configuration is more repulsive than that in the $4d^{10}$ configuration is as follows. We first note that the $5s$ orbital of Pd is more diffuse than the $4d$ orbital. The atomic radii $\langle r \rangle$ of the Hartree-Fock AO's of the ^3D (d^9s^1) state of Pd are[6]

$$\langle r \rangle_{4d} = 0.765 \text{ Å}, \quad \langle r \rangle_{5s} = 1.945 \text{ Å}$$

Since the $5s$ orbital is more diffuse than the $4d$ orbital, the electron in the $5s$ orbital is less able to shield its central nucleus than the electron in the $4d$ orbital, when the attacking H_2 molecule is not far away. Therefore, the Pd atom in the $4d^95s^1$ configuration is more repulsive than the Pd atom in the $4d^{10}$ configuration.

IV. CONCLUSION

We studied the interaction of the hydrogen molecule with the palladium atom in the singlet ground state ($4d^{10}, {}^1S$) and in the lowest triplet state ($4d^95s^1, {}^3D$), as a model of the chemisorption of the H_2 molecule on the Pd metal. We used the effective core potential method and calculated the accurate Hellmann-Feynman force of the H_2 system adding the first derivatives of the hydrogen basis set. We used an intuitive force concept for studying the origin of the interaction.

We found that the singlet Pd (^1S)—H_2 system is attractive but the triplet Pd (^3D)—H_2 system is repulsive. The side-on approach is found to be the preferable path. For the Pd (^1S)—H_2 system, the Pd—H bonds are gradually formed as the H_2 molecule approaches. The electron density is accumulated in the overlap region between H_2 and Pd and it causes the F (H_2—Pd) force which pulls the H_2 molecule onto the metal atom. As the hydrogen molecule approaches, the protons receive the force which prolongs the H—H distance. This is due to the decrease in the electron density in the bonding region of the two hydrogens. In an MO interaction picture, this reorganization of the electron density is due to an electron transfer from the bonding MO of the hydrogen molecule to the empty hybrid orbital of the $5s$, $5p_z$, and $4d_{z^2}$ AO's of the Pd atom. The back-transfer of electrons from the $4d_{yz}$ AO to the antibonding orbital of the H_2 molecule is small.

For the triplet Pd (^3D)—H_2 system, the electron density of the Pd atom is less affected by the approach of the H_2 molecule and tends to keep its spherical symmetry. Further, the Pd atom in the $4d^95s^1$ configuration is more repulsive than that in the $4d^{10}$ configuration. This is because the electron density in the $4d^95s^1$ configuration is less able to shield its Pd nucleus than the electron density in the $4d^{10}$ configuration, since the $5s$ orbital is more diffuse than the $4d$ orbital. Therefore, the H_2 molecule is repelled by the Pd atom.

REFERENCES

1. *The Palladium-Hydrogen System,* F. A. Lewis, New York, Academic Press, 1967.
2. D. M. Roundhill, *Adv. Organomet. Chem.* **13** (1975) 273; P. M. Henry, *Adv. Organomet. Chem.* **13** (1975) 273.
3. *The Organic Chemistry of Palladium,* Vols. 1, 2, P. M. Maitlis, New York, Academic Press, 1971.
4. *Advanced Inorganic Chemistry,* F. A. Cotton and G. Wilkinson, New York, John Wiley & Sons, 1980.
5. H. Basch and S. Topiol, *J. Chem. Phys.* **71** (1979) 802.
6. P. S. Bagus and C. Björkman, *Phys. Rev. A* **23** (1981) 461.
7. G. Pacchioni, J. Koutecký, and P. Fantucci, *Chem. Phys. Lett.* **92** (1982) 486.
8. S. W. Wang and K. S. Pitzer, *J. Chem. Phys.* **79** (1983) 3851.
9. *Molecular Spectra and Molecular Structure. IV Constants of Diatomic Molecules,* K. P. Huber and G. Herzberg, New York, Van Nostrand Reinhold Co., 1979.
10. A. A. Bagatur'yants, N. A. Anikin, G. M. Zhidomirov, and V. B. Kazanskii, *Russ. J. Phys. Chem. (Engl. Transl.)* **55** (1981) 1157.
11. L. R. Kahn, P. Baybutt, and D. G. Truhlar, *J. Chem. Phys.* **65** (1976) 3826.
12. P. J. Hay, *J. Amer. Chem. Soc.* **103** (1981) 1390.
13. H. Nakatsuji, *J. Amer. Chem. Soc.* **95** (1973) 345, 354, 2084; **96** (1974) 24, 30; H. Nakatsuji and T. Koga, *J. Amer. Chem. Soc.* **96** (1974) 6000; chapter 3 of reference 14.

14. *The Force Concept in Chemistry*, B. M. Deb (Ed.), New York, Van Nostrand Reinhold Co., 1981.
15. H. Nakatsuji, K. Kanda, and T. Yonezawa, *Chem. Phys. Lett.* **75** (1980) 340; H. Nakatsuji, T. Hayakawa, and M. Hada, *Chem. Phys. Lett.* **80** (1981) 94; H. Nakatsuji, K. Kanda, M. Hada, and T. Yonezawa, *J. Chem. Phys.* **77** (1982) 3109; **79** (1983) 2493.
16. H. Nakatsuji, M. Hada, and T. Yonezawa, *Chem. Phys. Lett.* **95** (1983) 573.
17. H. Nakatsuji, K. Kanda, and T. Yonezawa, *J. Chem. Phys.* **77** (1982) 1961; H. Nakatsuji, M. Hada, K. Kanda, and T. Yonezawa, *Int. J. Quantum Chem.* **23** (1983) 387; H. Nakatsuji and K. Kanda, in: J. P. Dahl and J. Avery (Eds.), *Local Density Approximations in Quantum Chemistry and Solid State Physics*, New York 1984, pp. 771—784.
18. T. H. Dunning, Jr., *J. Chem. Phys.* **53** (1970) 2823.
19. *Atomic Energy Levels*, Vol. III, C. E. Moore, Washington D. C., National Bureau of Standard, 1971.
20. M. J. S. Dewer, *Bull. Soc. Chim. Fr.* (1951) 79; J. Chatt and L. A. Duncanson, *J. Chem. Soc.* (1953) 2939.
21. K. Fukui and H. Fujimoto, *Bull. Chem. Soc. Japan*, **41** (1968) 1989; **42** (1969) 3399.

SAŽETAK

Interakcija molekule H_2 sa atomom paladija primjenom koncepta Hellmann-Feynmanove sile

Hiroshi Nakatsuji i Masahiko Hada

Kao model za kemisorpciju razmotrena je interakcija molekule H_2 i atoma Pd u singuletnom ^1S ($4d^{10}$) i tripletnom ^3D ($4d^9 5s^1$) stanju. Sila kojom atom Pd djeluje na H_2 izračunana je vrlo točno. Ustanovljeno je da je sila privlačna za singulet, a odbojna za triplet. Pri veznoj interakciji dolazi do gomilanja elektronske gustoće u regiji prekrivanja atoma Pd i molekule H_2, što se događa na račun smanjenja gustoće duž veze H—H. Pri tome se tvori nova veza Pd—H, a slabi veza između atoma vodika. Dolazi i do migracije naboja iz vezne MO H_2 u prazne $5s5p_z$ orbitale atoma Pd.